JOURNAL OF GEOPHYSICAL RESEARCH, VOL. 106, NO. C6, PAGES 11,731–11,742, JUNE 15, 2001

A 10 year intercomparison between collocated Special Sensor Microwave Imager oceanic surface wind speed retrievals and global analyses

T. Meissner, D. Smith, and F. Wentz
Remote Sensing Systems, Santa Rosa, California

Abstract. To evaluate the scalar ocean surface wind speeds obtained from the Special Sensor Microwave Imager (SSM/I), we compare them over the time period from July 1987 through December 1997 with those from two global analyses: the National Center for Environmental Prediction (NCEP)/National Center for Atmospheric Research (NCAR) Annual Reanlysis and the European Center for Medium-Range Weather Forecasts (ECMWF)/Tropical Ocean-Global Atmosphere Global Surface Analysis. We perform a statistical analysis for the whole globe and present time series analyses for selected geographical regions in connection with collocated wind speed difference maps. In order to evaluate further geographical biases observed in the SSM/I versus analyses comparisons we use wind speeds from the NASA scatterometer (NSCAT) for the 10 month period from September 1996 through June 1997 as a third data source. The value of the standard deviation for all collocated SSM/I − ECMWF wind speed differences is 2.1 m s^{-1} and for all collocated SSM/I − NCEP/NCAR reanalyis wind speed differences is 2.4 m s^{-1}. When taking monthly or yearly averages in each pixel, which has the effect of cancelling out small timescale wind speed fluctuations, the values are between 0.8 and 1.2 m s^{-1}, respectively. Global biases range between −0.05 and +0.55 m s^{-1} for the various SSM/I satellites. Our analysis allows us to identify regional biases for both the SSM/I and analyses winds. The NCEP/NCAR reanalysis wind speeds appear underestimated in the tropical Pacific and tropical Atlantic. ECMWF wind speeds appear underestimated near the southern Pacific islands NE of Australia. The analyses wind speeds are higher than the SSM/I wind speeds near the Argentinean coast. The SSM/I wind speeds appear high in the extratropical central and eastern Pacific and low in certain coastal regions with eastern boundary currents and in the Arabian Sea. The size of some of these biases are seasonally dependent.

1. Introduction

Data from satellite-borne microwave radiometers have become extremely useful and important for studying the Earth's climate. Their capability to measure simultaneously ocean surface wind speed, sea surface temperature, sea ice cover, and profiles of air temperature and atmospheric water (vapor, liquid, and ice) makes radiometers unique tools for investigating atmospheric and oceanographic processes. The results from radiometer measurements also provide an important input for numerical weather forecasting and general circulation models.

The main objective of this paper is to perform an evaluation of the ocean surface wind speeds measured by the Special Sensor Microwave Imager (SSM/I). The instrument is flown by the Defense Meteorological Satellite Program (DMSP) on successive polar orbiting platforms. Since July 1987, five SSM/Is have been receiving data (F08, F10, F11, F13, and F14). F08 and F10 stopped operating in December 1991 and November 1997, respectively. The SSM/I data are processed under NASA's scanning multichannel microwave radiometer (SMMR)-SSM/I Pathfinder program using an algorithm that is based on a model for the brightness temperature of the ocean and the intervening atmosphere using five channels (19 GHz v and h pol, 22 GHz v pol, and 37 GHz v and h pol) [*Wentz*, 1997]. The algorithm can simultaneously retrieve, with high precision, three geophysical parameters: wind speed 10 m above sea level, columnar water vapor, and columnar liquid cloud water. In addition, precipitation rate is inferred. The final data products are made available daily on Remote Sensing System's Web site (*http://www.ssmi.com*) and have become widely used in weather and climate research. A detailed and updated validation study of these products is therefore highly desirable.

In this study we compare the satellite wind speeds with those obtained from two widely studied global analyses: the NCEP/NCAR reanalysis [*Kalnay et al.*, 1996] and the ECMWF/TOGA Global Surface Analysis [*European Center for Medium-Range Weather Forecasts (ECMWF)*, 1993]. These two analyses were selected because they cover the whole time period for which the SSM/I data exist. The NCEP/NCAR reanalysis uses one single model without changes during the time period, whereas the ECMWF analysis has undergone various model changes since 1987. Both analyses provide wind speeds on a global grid at a 12 or 6 hour time resolution, respectively. In order to compare with satellite measurements it is necessary to perform appropriate collocations and to average out small-scale fluctuations.

We have also included in this study wind speeds from the

Paper number 1999JC000098.
0148-0227/01/1999JC000098$09.00

NASA scatterometer (NSCAT), which received data over a 10 month period from September 1996 through June 1997. Despite this limited time period the NSCAT measurements provide crucial information for our study in that they serve as a third data source, which can help us to determine if certain biases are due to inaccuracies of either the SSM/I or the analyses winds. In this manner we identify shortcomings in both the satellite data and the analyses data.

Earlier studies that compared satellite and ECMWF ocean surface wind speed data were performed by *Halpern et al*. [1994] for the time period 1988–1991 and by *Boutin et al*. [1996] for the time period 1987–1992. The SSM/I data in these papers were derived using an older version of the current Pathfinder algorithm. Our study confirms some of their results but also exhibits various new effects.

Our paper is organized as follows: Section 2 contains short descriptions of the various data sets, quality check, and collocation procedures. Section 3 reports results of a global statistical analysis of the wind differences between SSM/I, the analyses, and NSCAT. We compare the SSM/I instruments with each other, identify a drift in the morning overpass of F10, and calculate averages and standard deviations of the global wind speed differences. Section 4 presents long time series in specific latitudinal bands and collocated seasonal wind speed difference maps, using F11 data as an example. This enables us to identify various geographical regions and time periods, where either the SSM/I or the analyses wind speeds are too high or too low. Section 5 provides a short summary. A list of all abbreviations and notations used in this paper can be found at the end.

2. Study Data

The SSM/I data used in this study are produced under NASA's Pathfinder program by a unified physically based algorithm. This algorithm has been used for processing all SSM/I data, and the entire series of SSM/Is has been intercalibrated at the antenna temperature level. In order to validate the SSM/I wind speeds they have been collocated to in situ measurements from buoys. One finds a bias of 0.3 m s^{-1} and a standard deviation of 0.9 m s^{-1} for the SSM/I − buoy wind speed difference as long as pixels are excluded for which the algorithm detects rain [*Mears et al*., this issue; *Wentz*, 1997]. The mapped wind speeds on this public data set are stored in increments of 0.15 m s^{-1} on a 0.25° × 0.25° grid (1440 × 720 pixels). Furthermore, they are separated into morning and evening overpasses (descending and ascending swaths). At higher latitudes where several observations fall into one pixel the data have been averaged. The separation into ascending and descending swaths allows for study of diurnal effects as well as of effects that depend on the radiometer looking azimuth relative to the wind direction. We extended our analysis only through December 31, 1997, because at the time when our study was performed the National Centers for Environmental Prediction (NCEP)/National Center for Atmospheric Research (NCAR) reanalysis was available only until that date. We excluded observations from F14, which started operating in May 1997. The analysis time for the individual satellites are July 1987 to December 1991 (F08), January 1991 to November 1997 (F10), January 1992 to December 1997 (F11), and May 1995 to December 1997 (F13).

A strict quality check was imposed on the satellite data in order to remove rain, land, and ice. We excluded any pixel if one of the following conditions were met in the pixel or in any of the eight adjacent pixels: (1) Rain was present. (2) The retrieved liquid cloud water was more than 0.2 mm [*Wentz*, 1997]. (3) The pixel was over land or ice. The second condition was imposed to avoid undetected rain. The exclusion of the eight adjacent pixels was done to prevent nearby rain, land, or ice from influencing the measured brightness temperature, which could affect the retrieved wind speed. It also avoids cases where either the land or the ice mask is inaccurate.

The NCEP/NCAR reanalysis [*Kalnay et al*., 1996] is available from the NCAR data support section on CD-ROMS. The time and space resolutions of the scalar wind speeds are two times daily (0000 and 1200 UT) on a T62 Gaussian grid (192 × 96). The longitudinal spacing is regular at 1.875°. A regular grid spacing of 1.904° between 88.536°S and 88.536°N can approximate the latitudinal grid spacing. The maximal deviation between these regular latitudes and the original Gaussian latitudes is 0.03°. The time and space resolution of the *ECMWF* [1993] data is four times daily (0000, 0600, 1200, and 1800 UT) on an N80 Gaussian grid (320 × 160). This grid has a regular longitudinal spacing of 1.125°. We approximate the latitudes by a regular spacing of 1.121° between 89.141°S and 89.142°N, which has a maximal error of 0.0147°. Note that the ECMWF model has undergone various changes during the time period under consideration, whereas the NCEP/NCAR reanalysis winds are from one single model. Both the NCEP/NCAR and the ECMWF winds are given at 10 m above sea level. In order to collocate the analyses data with the satellite data in time and space we used a simple trilinear interpolation for longitude, latitude, and time.

The NSCAT instrument operated on the ADEOS 1 platform for a 10 month period. The satellite was launched on August 17, 1996, and suffered a solar panel failure on June 29, 1997. NSCAT ocean wind vectors at 10 m height are derived from backscatter measurements using the NSCAT 2 model function, which is an improved version of the NSCAT 1 model function [*Wentz and Smith*, 1999]. NSCAT high-resolution merged data are provided as 25 km wind vector cells across two 600 km wide instrument measurement swaths [*Dunbar*, 1997]. The equatorial crossing time of NSCAT (1040/2240 UT) was ~20 min after the F10 SSM/I equatorial crossing time (1020/2220 UT). This provided a sufficiently large number of collocations for data analysis. NSCAT and SSM/I collocations were obtained by selecting the SSM/I grid cell containing the NSCAT footprint and choosing the SSM/I wind speed for that cell that was closest in time to the NSCAT measurement. The observation was excluded if the SSM/I observation was made >30 min from the NSCAT observation time. In addition, no collocation was done if rain was present within the SSM/I cell or any of the eight surrounding SSM/I cells or if the cloud liquid water was >0.2 mm. Approximately 3.5×10^7 or 30% of all NSCAT wind vector measurements were successfully collocated with F10 SSM/I measurements. Compared with buoy observations, the quality of the NSCAT wind speed is comparable to the quality of the SSM/I wind speeds. If collocated with buoy observations, one finds a mean of +0.15 m s^{-1} and a standard deviation of 1.26 m s^{-1} for the NSCAT − buoy wind speeds. NSCAT data were also collocated with the ECMWF and NCEP/NCAR data described above. Both were trilinearly interpolated to the NSCAT location and time.

Finally, we want to note that neither of the global analyses (NCEP/NCAR or ECMWF) has assimilated any of the satellite wind speed products that we consider in our study (SSM/I

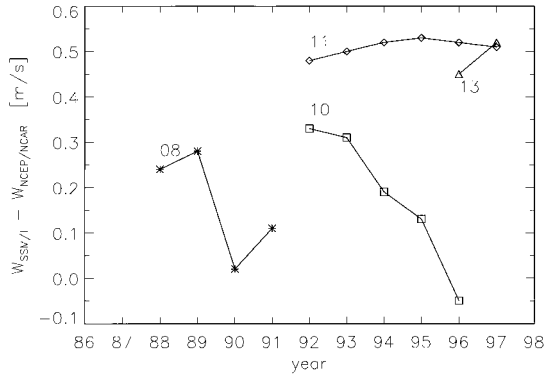

Figure 1. Yearly averages of collocated wind speed differences $W_{\mathrm{SSM/I}} - W_{\mathrm{NCEP/NCAR}}$ between the four SSM/I satellites and the NCEP/NCAR reanalysis.

or NSCAT). Though the NCEP/NCAR reanalysis incorporates ocean surface wind speeds from SSM/I [*Kalnay et al*., 1996], those wind speeds are derived using a neural network algorithm [*Krasnopolsky et al*., 1995] and are a completely different product than the Pathfinder algorithm [*Wentz*, 1997] wind product used in this study. It is therefore meaningful to draw an intercomparison between the various products of our study.

3. Global Statistical Results

3.1. Comparison Between the SSM/I Satellites

We have performed a comparison of wind speed data from four SSM/I satellites F08, F10, F11, and F13 to the NCEP/NCAR reanalysis winds. Since these SSM/I data span a time period of >10 years, the NCEP/NCAR reanalysis winds were selected for comparison. Unlike ECMWF winds, the NCEP/NCAR reanalysis winds have been consistently processed with one model throughout the considered time period. Figure 1 displays the global yearly average wind speed differences for the SSM/I satellites that were derived from data collocated over the global oceans. In order to avoid samples that do not contain a full year of data or that contain years with large blackout periods we have omitted SSM/I data from 1987 for F08, 1991 and 1997 for F10, and 1995 for F13. Each global yearly average in Figure 1 has been computed from a large number of data ($N \approx 10^8$).

As we will discuss in section 3.2 in more detail, the distribution of the wind speed differences between SSM/I and the NCEP/NCAR reanalysis is approximately Gaussian with a standard deviation of $\sigma \approx 2.4$ m s^{-1}. The standard error of the data points in Figure 1 is $\sim\sigma/\sqrt{\mathrm{N}}$, which is extremely small. Consequently, any difference between two of these points has to be regarded as statistically significant. In other words, the probability that the differences between two of the points can be attributed to noise in the single measurements of the wind speed differences is zero.

The wind speed differences for SSM/I satellites lie within a 0.6 m s^{-1} range. Originally, the first SSM/I satellite, F08, was calibrated using satellite-buoy overpasses [*Wentz*, 1997]. Then each successive satellite was calibrated to the previous one, F10 was calibrated to F08, F11 was calibrated to F10, and F13 was calibrated to F11. Ideally, all SSM/Is would show the same wind speed difference with regard to NCEP/NCAR reanalysis data, and those differences would change little over time. However, two factors result in this not being the case. First, small errors in intercalibrating the satellites at the antenna temperature level yield small differences between the SSM/I satellite wind speed differences. For example, the F11 wind speed difference value for 1992 in Figure 1 should match F10 for that year if F11 had been exactly intercalibrated to F10. Second, while in case of F11 the yearly average wind speed differences stay almost constant over time, as we would ideally expect, two satellites, in particular, show fluctuations in the wind speed comparison, F08 and F10. This fluctuating wind speed difference is confirmed by a recent study [*Mears et al*., this issue], which found a very similar behavior for the time dependence of the SSM/I − buoy wind speed differences. We therefore have to attribute the time-dependent changes or fluctuations to the SSM/I wind speeds and not to the NCEP/NCAR reanalysis wind speeds.

In the case of F10 the yearly global wind speed difference systematically decreased from 0.33 m s^{-1} in 1992 to −0.05 m s^{-1} in 1996. The effect is strongest for the morning overpass, where $\langle W_{\mathrm{F10M}} - W_{\mathrm{NCEP/NCAR}} \rangle$ decreased by more than 0.45 m s^{-1} between 1992 and 1996. Since the F10 satellite platform was misplaced in orbit, the orbit drifted during the time of operation. The orbital drift produced changes in the equatorial crossing time of the descending/ascending orbit. The crossing time changed from about 0800/2000 UT in 1991 to about 1020/2220 UT by late 1996. This resulted in observation of meteorological parameters, such as atmospheric profiles of temperature, water vapor, and clouds or surface wind speeds, at a later time. The retrieval algorithm for the SSM/I wind speed retrieval [*Wentz*, 1997] is based on a model function for the measured brightness temperatures. This model function is derived from the theory of radiative transfer and depends on these meteorological parameters. A systematic change in these meteorological parameters due to a change in the equatorial crossing time will therefore influence the SSM/I wind speed retrievals.

The F08 SSM/I yearly average wind speed difference decreases by about 0.25 m s^{-1} from 1989 to 1990 and then increases again by about 0.1 m s^{-1} in 1990. Looking at the values for the average yearly global wind speeds, we find that $\langle W_{\mathrm{F08}} \rangle$ was 7.36 m s^{-1} in 1988, 7.34 m s^{-1} in 1989, and 7.07 m s^{-1} in 1990. In comparison, the values for $\langle W_{\mathrm{NCEP/NCAR}} \rangle$ were 7.12 m s^{-1} in 1988, 7.06 m s^{-1} in 1989, and 7.05 m s^{+1} in 1990. This confirms that the observed change in wind speed difference is primarily due to F08. It could, again, be caused by an orbital drift of the satellite or also by some climate fluctuations, which could have influenced the meteorological conditions in the yearly global sample. Another cause could be geolocation errors, such as the reported Earth incidence angle. However, we are not aware that any of these effects occurred in this case. We currently do not have an explanation for the observed behavior of F08.

For the following sections we have chosen F11 as a representative example of the SSM/I instruments. It has a long operational period available for analysis (January 1992 to December 1997) and, as we have seen, no fluctuation in wind speed difference. A full data analysis shows that all statistical and geographical features are both qualitatively and quantitatively the same for the four satellites, aside from the small offsets of the global wind speeds, as shown in Figure 1. Despite the orbital drift problems with F10 we also included a short 10 month study of F10 SSM/I data in our analysis because of its optimal collocation with NSCAT. However, because of the substantial diurnal meteorological effect in the morning over-

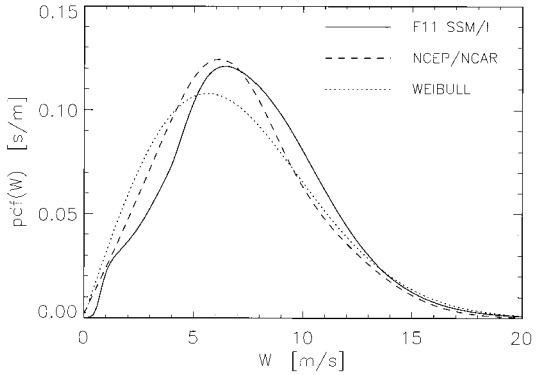

Figure 2. Probability density functions of wind speeds W (pdf (W)) obtained from the SSM/I satellite F11 (solid line) and the NCEP/NCAR reanalysis (dashed line) between January 1992 and December 1997. The bin size for the wind speeds is 0.15 m s^{-1}. For comparison, a quadratic Weibull distribution with $\langle W \rangle = \langle W_{\mathrm{NCEP/NCAR}} \rangle = 7.0$ m s^{-1} (dotted line) is also shown.

pass data, we included only the evening overpass data from F10 and NSCAT data and discarded morning overpass data.

3.2. Detailed Description of F11 SSM/I Wind Speed Comparison

Figure 2 shows the probability density functions (pdfs) of all collocated wind speeds from the F11 SSM/I (solid line) and the NCEP/NCAR reanalysis (dotted line) over the whole globe between January 1992 and December 1997. This analysis produced $\sim N \approx 6 \times 10^8$ events. We used 0.15 m s^{-1} bins for the SSM/I data. The statistical distribution of the ECMWF winds is almost identical to that of the NCEP/NCAR reanalysis winds and therefore is not shown. The global and time-averaged wind speeds are $\langle W_{\mathrm{F11}} \rangle = 7.55$ m s^{-1}, $\langle W_{\mathrm{NCEP/NCAR}} \rangle = 7.04$ m s^{-1}, and $\langle W_{\mathrm{ECMWF}} \rangle = 7.15$ m s^{-1}. The biases between the global satellite and analyses winds are $\langle W_{\mathrm{F11}} - W_{\mathrm{NCEP/NCAR}} \rangle = 0.51$ m s^{-1} and $\langle W_{\mathrm{F11}} - W_{\mathrm{ECMWF}} \rangle = 4.0$ m s^{-1}, respectively. Note that the global average of the analyses wind speeds would be $\sim$1.0–1.2 m s^{-1} larger if 1000 mbar winds were used instead of the 10 m winds used in this study. The distribution of the global wind speeds is approximately following a quadratic Weibull function [*Wilks*, 1995]:

$$\mathrm{pdf}_{\mathrm{Weibull}}(W)dW = \frac{1}{\delta^2}\, e^{-w^2/2\delta^2} W dW, \qquad (1)$$

which peaks at $W_{\max} = \delta$ and has a mean of $\langle W \rangle = \sqrt{\pi/2}\ \delta \approx 1.25\delta$ and a standard deviation of $\sigma(W) = \sqrt{2-\pi/2}\ \delta \approx 0.66\delta$. The form (1) can be obtained from the joint pdf of normal (Gaussian) distributed zonal and meridional wind components if one assumes that their widths are direction-independent and integrates over wind direction. For comparison, we have included a distribution of the form (1) whose average wind speed is equal to $\langle W_{\mathrm{NCEP/NCAR}} \rangle = 7.04$ m s^{-1} in Figure 2 (dotted line).

Figure 2 also shows that for higher wind speeds $W \geq 7$ m s^{-1}, there is a tendency for higher satellite wind speeds than analyses wind speeds, whereas the opposite occurs for lower wind speeds $W \leq 7$ m s^{-1}. This feature has presumably its origin in the SSM/I wind speed retrieval algorithm. As we discussed in section 3.1, this algorithm is based on a model function $T_{B_{\mathrm{model}}}(W, \ldots)$ for the brightness temperature measured by the satellite, which is derived from a radiative transfer model and depends on the wind speed W. It is known from other instruments [*Wentz and Smith*, 1999] that even small uncertainties in the derivative $\partial T_{B\mathrm{model}}/\partial W$ can distort the wind speed histogram and lead to modes such as the one exhibited in Figure 2.

The standard deviations of the wind speed differences over the whole sample spaces are $\sigma(W_{\mathrm{F11}} - W_{\mathrm{NCEP/NCAR}}) = 2.4$ m s^{-1} and $\sigma(W_{\mathrm{F11}} - W_{\mathrm{ECMWF}}) = 2.1$ m s^{-1}, respectively. The value for the ECMWF winds is slightly smaller than that for the NCEP/NCAR reanalysis winds and could, to some extent, be attributed to the higher space and time resolution of the ECMWF data. The better resolution of ECMWF data reduces the error in the space and time collocation. It could also be an indication that the ECMWF analysis itself is slightly more accurate than the NCEP/NCAR reanalysis or that the data going into the ECMWF assimilation are of better quality than the ones going into the NCEP/NCAR reanalysis.

Figure 3 shows the pdf of the wind speed differences $\Delta W = W_{\mathrm{F11}} - W_{\mathrm{NCEP/NCAR}}$ between 1992 and 1997. We have shifted the curve by its mean value $\langle \Delta W \rangle = 0.51$ m s^{-1} so that it is centered at the origin. As we can see, pdf (ΔW) is close to a normal (Gaussian) distribution that is centered at the origin and has a width of $\sigma(\Delta W) = 2.4$ m s^{-1}.

The analyses provide averages of wind speed only within their spatial and temporal resolution. Despite the fact that we interpolate the analyses events to the satellite events we cannot perform a true collocation since the analyses do not provide real measurements. From in situ measurements we know that wind speeds have a large variability on timescales of 1 hour [*Wells*, 1997]. It is therefore not surprising that the standard deviations of the SSM/I analyses wind speed differences listed in section 3.2 are noticeably larger than standard deviations from the collocation of two real-time events. For example, the comparison of SSM/I and in situ buoy wind speeds [*Mears et al*., this issue] finds a standard deviation of about 1.3 m s^{-1}.The SSM/I analyses standard deviations do not really give any information about the precision of either the satellite or the analyses wind speeds. Instead, to a large extent they reflect the

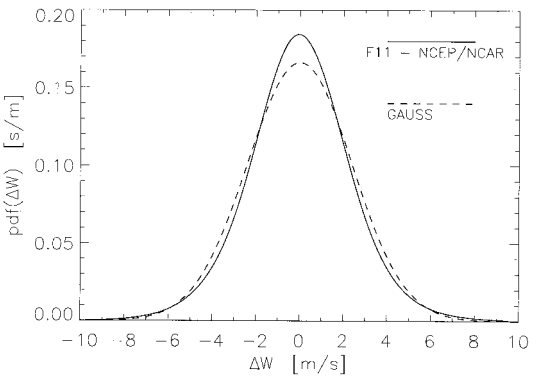

Figure 3. Probability density functions pdf (ΔW) of the wind speed differences ΔW between SSM/I F11 and the NCEP/NCAR reanalysis for the time between January 1992 and December 1997 (solid line). The bin size for the wind speeds is 0.15 m s^{-1}. The curve has been shifted by the value of the overall bias $\langle \Delta W \rangle = 0.5$ m s^{-1}, so that it is centered at the origin. For comparison, a Gaussian distribution centered at the origin with a width of $\sigma(\Delta W) = 2.4$ m s^{-1} is also shown (dashed line).

Table 1. Global Mean and Standard Deviation Wind Speed Differences Between SSM/I (F10E), NSCAT, NCEP/NCAR, and ECMWF[a]

	F10E − NSCAT	NSCAT − NCEP/NCAR	NSCAT − ECMWF	F10E − NCEP/NCAR	F10E − ECMWF
$\langle W \rangle$	0.28	05	−0.07	0.33	0.21
$\sigma(W)$	1.25	2.22	1.65	2.36	1.85
$\sigma(\bar{W})$	0.49	0.69	0.46	0.87	0.65

[a]Data are collocated over the 10 month period September 1996 to June 1997. Collocation was performed with respect to NSCAT evening overpasses. Here $\langle W \rangle$ denotes the average wind speed difference, $\sigma(W)$ denotes the standard deviation for all collocated events, and $\sigma(\bar{W})$ denotes the standard deviation after taking the time average over the 10 month period in each pixel. Units are m s^{-1}.

high variability of the wind speeds on timescales smaller than the analyses temporal resolutions. In order to obtain a better measure of the actual wind speed precision we average time-collocated events in each pixel over timescales large enough to cancel out the short timescale fluctuations. By using time-averaged wind speed differences for each grid pixel the standard deviations significantly decrease. The monthly time-averaged statistics for the wind speed difference between F11 SSM/I and the NCEP/NCAR reanalysis has a standard deviation of $\sigma(\bar{W}_{\mathrm{F11}} - \bar{W}_{\mathrm{NCEP/NCAR}}) = 1.0$–$1.2$ m s^{-1}, and for the wind speed difference between F11 and ECMWF we find $\sigma(\bar{W}_{\mathrm{F11}} - \bar{W}_{\mathrm{ECMWF}}) = 0.9$–$1.1$ m s^{-1}. For yearly averaged statistics we find $\sigma(\bar{W}_{\mathrm{F11}} - \bar{W}_{\mathrm{NCEP/NCAR}}) = 0.9$–$1.0$ m s^{-1} and $\sigma(\bar{W}_{\mathrm{F11}} - \bar{W}_{\mathrm{ECMWF}}) = 0.8$–$1.0$ m s^{-1}. An earlier analysis by *Boutin et al*. [1996], which compared ECMWF and SSM/I wind speeds, obtained standard deviations which were about 0.2 m s^{-1} smaller. This small difference can be explained by the fact that *Boutin et al*. [1996] used a previous version of the data and, furthermore, a different spatial collocation. They averaged the satellite measurements to the lower ECMWF resolution rather than interpolate the analyses winds to the higher satellite resolution as we have done in this study.

3.3. NSCAT and F10E Global Wind Comparison

We decided to include in this study a statistical analysis comparing NSCAT, SSM/I (F10E), NCEP/NCAR, and ECMWF wind speeds. Though the analysis consisted of fewer data because of limited NSCAT operation, we found the additional instrument-to-instrument comparison helpful in highlighting possible causes of the biases described in section 4. Table 1 contains global mean wind speed differences, standard deviations for all collocated events, and standard deviations after performing the time average in each pixel. Note that the F10 SSM/I events used for these statistics comprise only measurement times collocated to the NSCAT observations and only local evening data due to the orbital drift of the F10 SSM/I satellite. Therefore fewer than 15% of the NSCAT measurements are included in the analysis.

The very small biases between the NSCAT winds and both analyses winds (Table 1) are due to the fact that ECMWF wind speeds have been used for tuning the NSCAT model function [*Wentz and Smith*, 1999]. We also find that the value for $\langle W_{\mathrm{NSCAT}} - W_{\mathrm{NCEP/NCAR}} \rangle$ is about 0.1 m s^{-1} larger than the value for $\langle W_{\mathrm{NSCAT}} - W_{\mathrm{ECMWF}} \rangle$. This is in accordance with an observation from section 3.2 for F11. We attribute this difference to a genuine small difference between the two global analyses. In other words the ECMWF winds are about 0.1 m s^{-1} higher than the NCEP/NCAR winds. The value for the bias $\langle W_{\mathrm{F10E}} - W_{\mathrm{NSCAT}} \rangle$ is 0.28 m s^{-1}, which is consistent with the average difference between the F10E and the analyses wind speeds during September 1996 to June 1997. For the standard deviations σ (W) we obtain the smallest value in case of the F10E − NSCAT wind speed difference. This reflects partly the fact that for the two satellite measurements one can perform the most accurate time collocation. Another reason might be that the data analysis that is used within the global analyses consists of merging data by weighting model output (shorts-term forecasts) with observations. The model output as well as the observations may have biases with respect to the true values.

4. Regional and Seasonal Wind Speed Biases

4.1. Time Series of Specific Latitudinal Bands

Figure 4 shows monthly wind speed averages for F11 SSM/I (solid line), NCEP/NCAR reanalysis (dashed line), and ECMWF (dotted line) in five latitudinal bands (30°–80°N), (10°–30°N), (10°S–10°N), (30°–10°S), and (80°–30°S), which were obtained from collocated data. The monthly biases F11-NCEP/NCAR (dashed) and F11-ECMWF (dotted) are shown in Figure 5. The SSM/I to ECMWF biases shown tend to be smaller than the SSM/I to NCEP/NCAR wind speed biases.

At high latitudes a clear seasonal pattern is present in the mean wind speeds (Figures 4 (top) and 4 (bottom)). High wind speeds occur during December, January, and February at high northern latitudes and during the June, July, and August at high southern latitudes. The peak monthly average wind speeds are ~9.5 m s^{-1}, which is more than 2 m s^{-1} above the global average $\langle W \rangle = 7.5$ m s^{-1}. This seasonal signal is more than twice as strong in the Northern Hemisphere than in the Southern Hemisphere.

Within the northern latitudinal band (30°–80°N) the high wind speeds during the winter months lead, in turn, to large positive biases (Figure 5). This is consistent with the observation made from Figure 2 that at high wind speeds, SSM/I winds are higher than the analyses winds. During lower wind speed months the biases between SSM/I and analyses wind speeds are small or negative, and overall, the wind speed differences rarely exceed 1 m s^{-1} in either direction. This seasonal variation of the wind speed biases is also visible at middle northern latitudes (10°–30°N) but is weaker. At middle southern latitudes the bias of F11 with respect to NCEP/NCAR lies between 0.5 and 1.0 m s^{-1}, close to the global average, which is about 0.5 m s^{-1}. The bias between F11 and ECMWF lies above 1 m s^{-1} before late 1995 and drops to below 1 m s^{-1} after 1995, which can presumably be attributed to improvements in the ECMWF analysis (A. Hollingsworth, personal communication, 1999). In neither case is a seasonal signal visible. At high

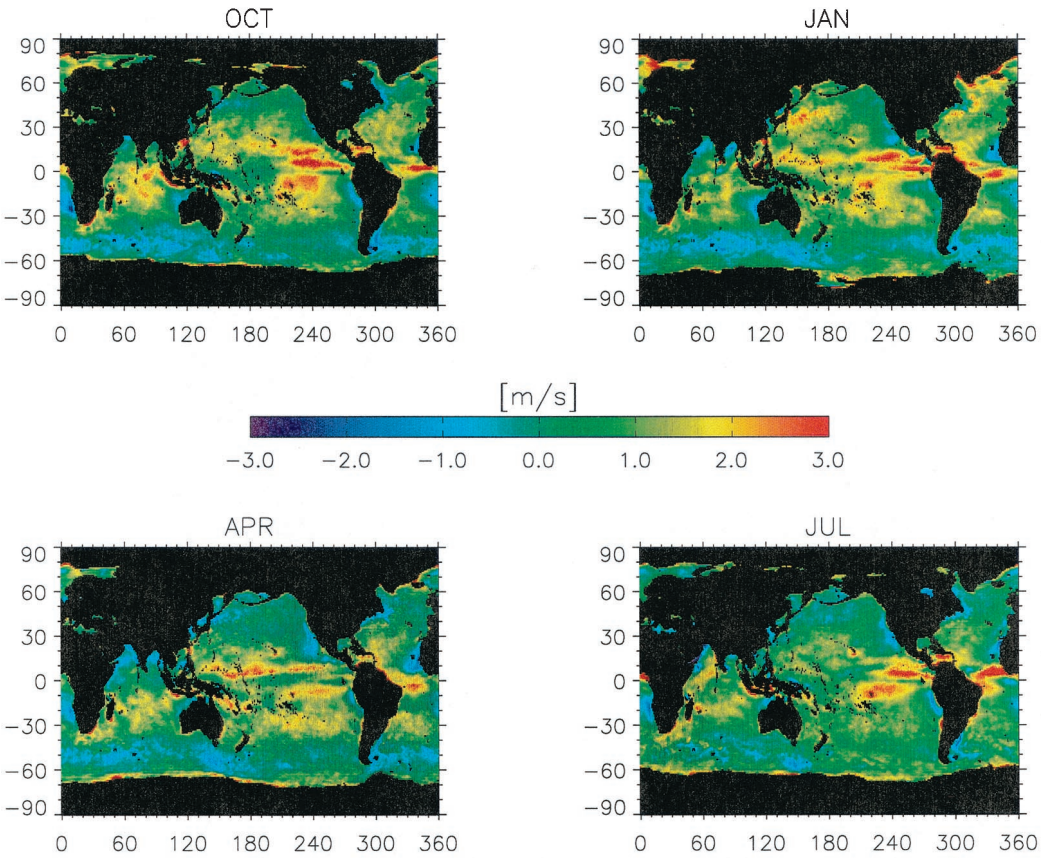

Plate 1. Maps of monthly averaged wind speed differences between F11 SSM/I and the NCEP/NCAR reanalysis for October, January, April, and July taken over the time period between 1992 and 1997. Pixels with <40 events have been blackened out.

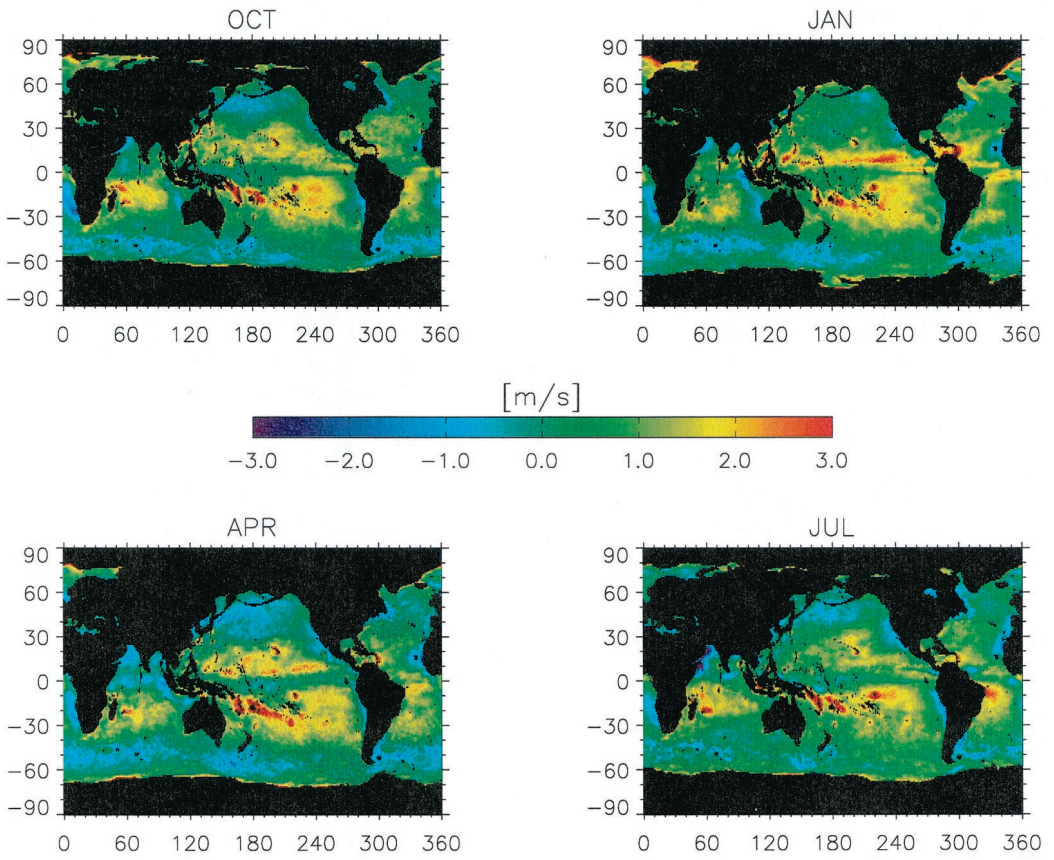

Plate 2. Maps of monthly averaged wind speed differences between F11 SSM/I and ECMWF for October, January, April, and July taken over the time period between 1992 and 1997. Pixels with <40 events have been blackened out.

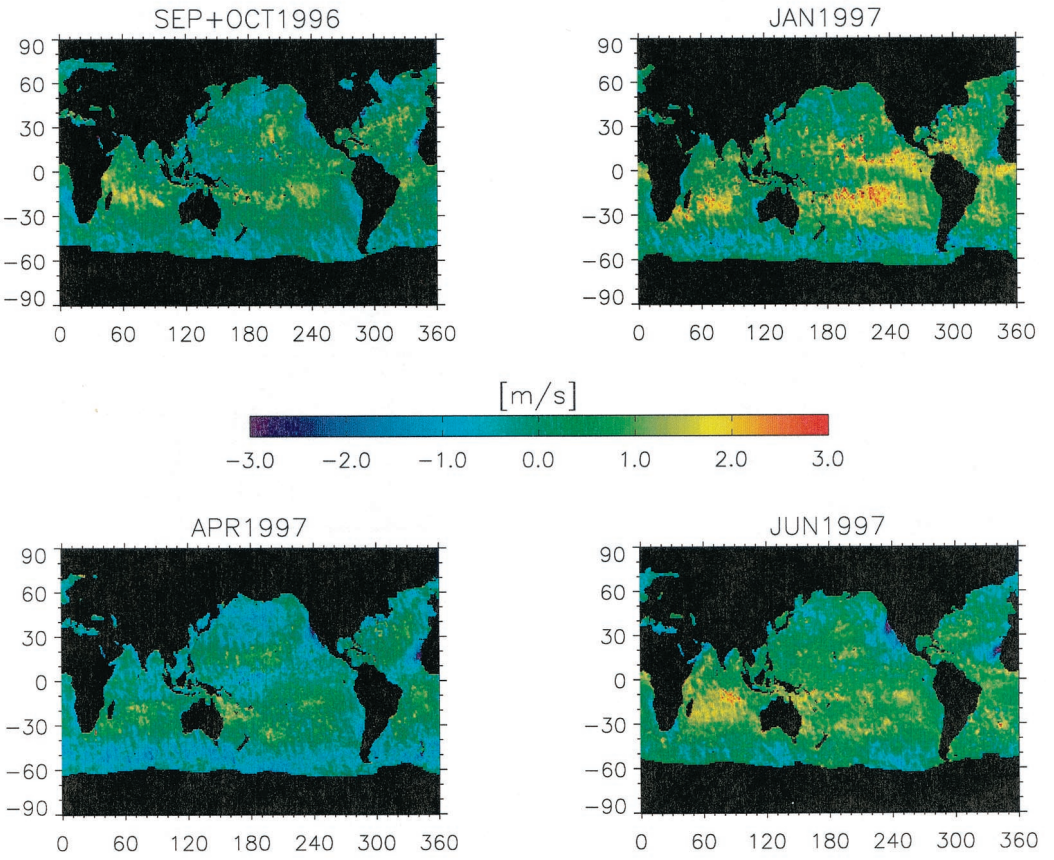

Plate 3. Population map (number of events) for Plates 1 and 2. Pixels with <40 events have been blackened out.

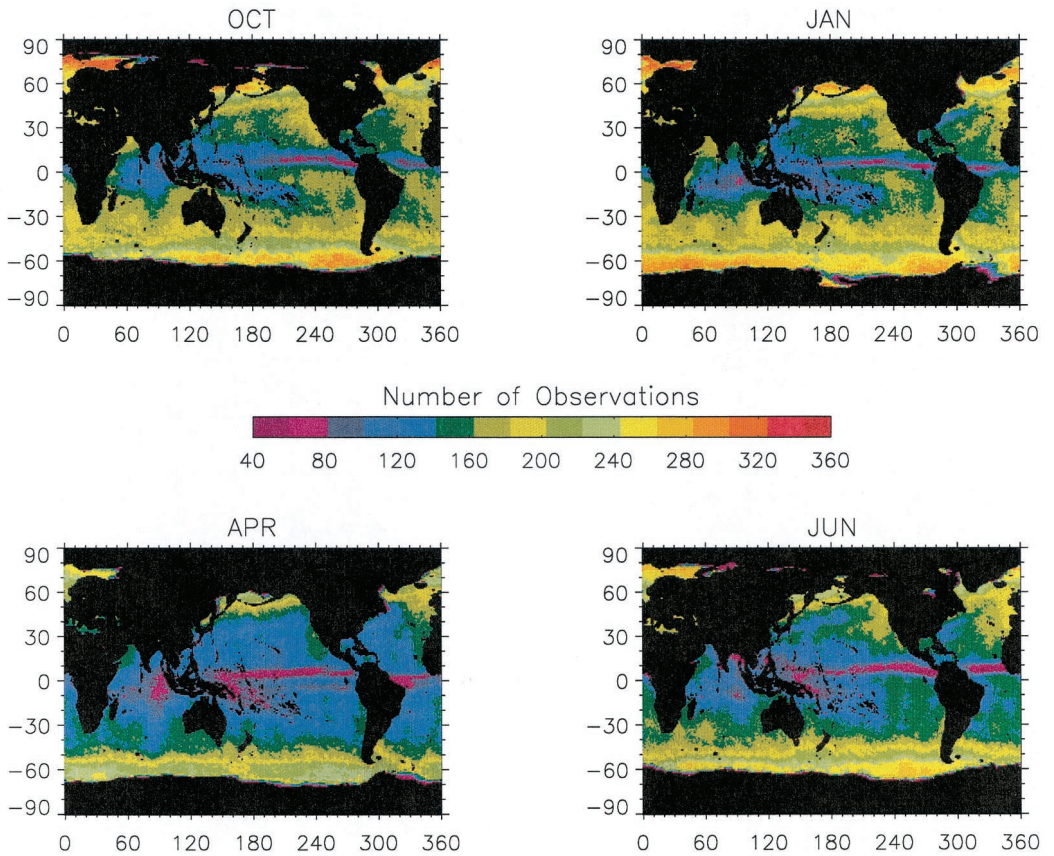

Plate 4. Maps of averaged wind speed differences between F10E SSM/I and NSCAT for September and October 1996, January 1997, April 1997, and June 1997.

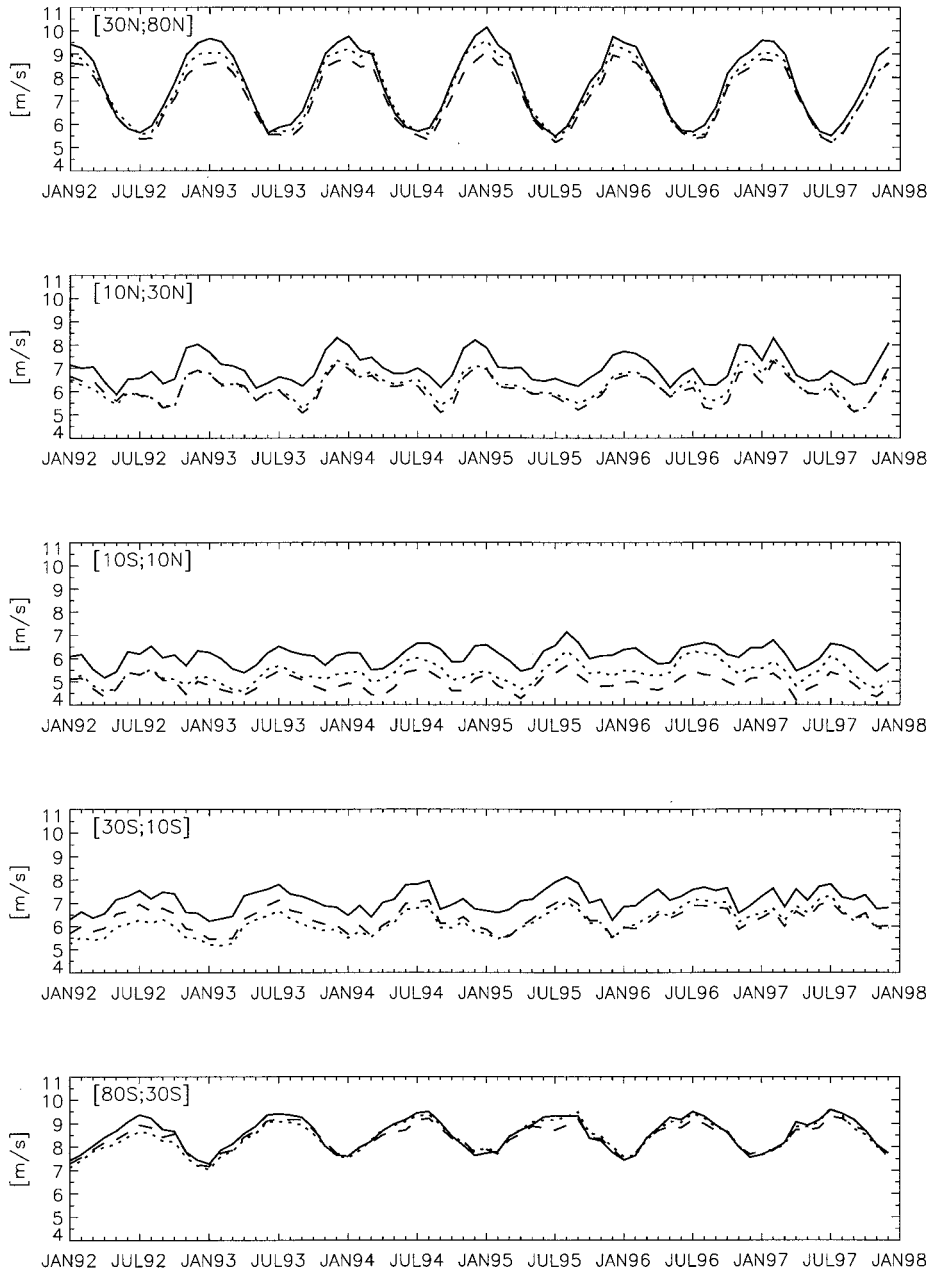

Figure 4. Monthly averaged wind speeds for the SSM/I satellite F11 (solid line), the NCEP/NCAR reanalysis (dashed line) and ECMWF (dotted line) in five latitudinal bands.

southern latitudes (80°–30°S) the wind speed biases are surprisingly small (<0.5 m s^{-1}). They show the same seasonal oscillation as is observed in the Northern Hemisphere but with a lower amplitude. We will come back to this point in section 4.2.

In the tropical region (10°–10°N) the NCEP/NCAR reanalysis winds are substantially lower than the SSM/I winds and remain so by ~ -1.0 to -1.5 m s^{-1}. In the case of ECMWF winds the biases in the tropical region are much smaller, between 0.5 m s^{-1} and 1.0 m s^{-1} and have therefore about the same size as the global bias. We conclude that the NCEP/NCAR reanalysis underestimates the true wind speeds in those regions.

Changes made in the ECMWF analysis during the second half of 1993 are visible in the time series (A. Hollingsworth, personal communication, 1999). The difference between the satellite winds and ECMWF winds decreased after that time at nearly all latitudes.

4.2. Collocated Difference Maps

Maps of the collocated monthly wind speed differences F11 − NCEP/NCAR (Plate 1) and F11 − ECMWF (Plate 2) show the location of regional biases. In order to demonstrate seasonal effects we chose to map four representative months, October, January, April, and July. For each map the 1° pixel averages were calculated from 1992 to 1997. Plate 3 shows the population map for Plates 1 and 2 displaying the number of collocated events in each pixel. In Plates 1–3, pixels with <40 events have been blackened out. We see that even in the tropics, where many data are omitted because of the precipi-

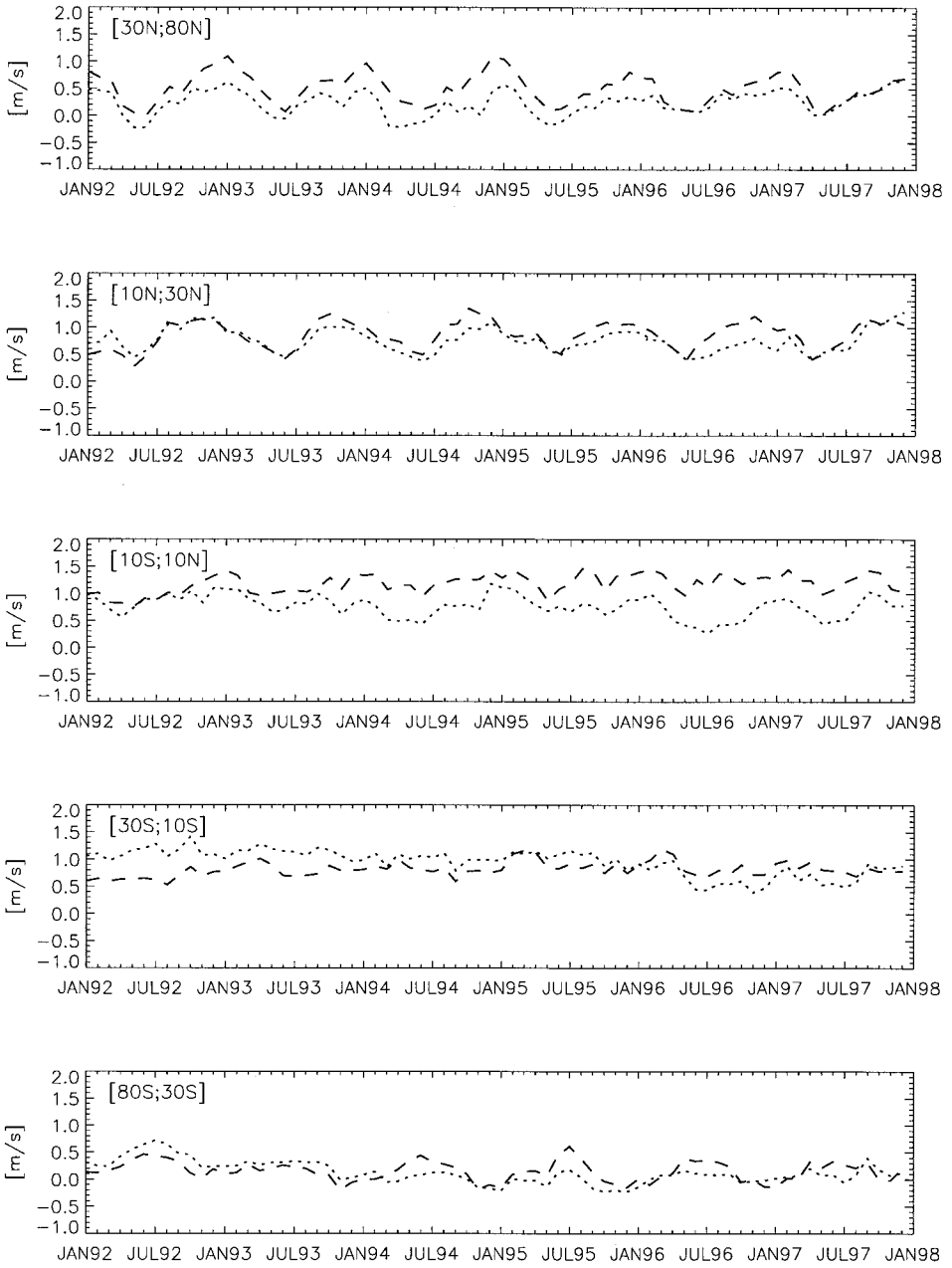

Figure 5. Monthly averaged wind speed differences in five latitudinal bands: F11 SSM/I − NCEP/NCAR (dashed line) and F11 SSM/I − ECMWF (dotted line).

tation filter, the number of events, N, very rarely drops below 50, which is large enough to keep the noise small. With $\sigma(W_{\mathrm{SSM/I}} - W_{\mathrm{NCEP/NCAR}}) \approx 2.5$ m s^{-1} (see section 3.2) the values for the noise $\sigma/\sqrt{\mathrm{N}}$ is about 0.35 m s^{-1} for $N = 50$ and about 0.13 m s^{-1} for $N = 372$, which is the highest possible value for N. In Plate 4 we provide F10E SSM/I − NSCAT collocated wind speed difference maps. Because of the relatively sparse number of collocated data available during the first few months of NSCAT operation (fall 1996), we chose to represent the four seasons with September and October 1996, January 1997, April 1997, and June 1997. The data include only measurements collected during the evening overpasses, where the orbit is ascending. Inspection shows that some of the same regional biases described below are present in these data despite the significantly fewer number of collocations.

The F11 − NCEP/NCAR wind speed bias demonstrated in the time series analysis is present in the maps of Plate 1. The NCEP/NCAR reanalysis underestimates the wind at tropical latitudes, especially in the eastern tropical Pacific and the Atlantic, where F11 SSM/I − NCEP/NCAR wind speed differences are as large as 3 m s^{-1}. The bias is lowest during spring (April). This again coincides with the time series analysis (Figure 5), which shows the lowest wind speed difference values for F11 − NCEP/NCAR mostly during the spring months. The effect is much smaller or not present, in the case of the F11 − ECMWF wind speed differences shown in Plate 2. *Boutin et al*. [1996] found that before 1989 the biases between SSM/I and the ECMWF wind speeds were much larger in these tropical regions. They found that the situation improved significantly after changes in the ECMWF analysis had been

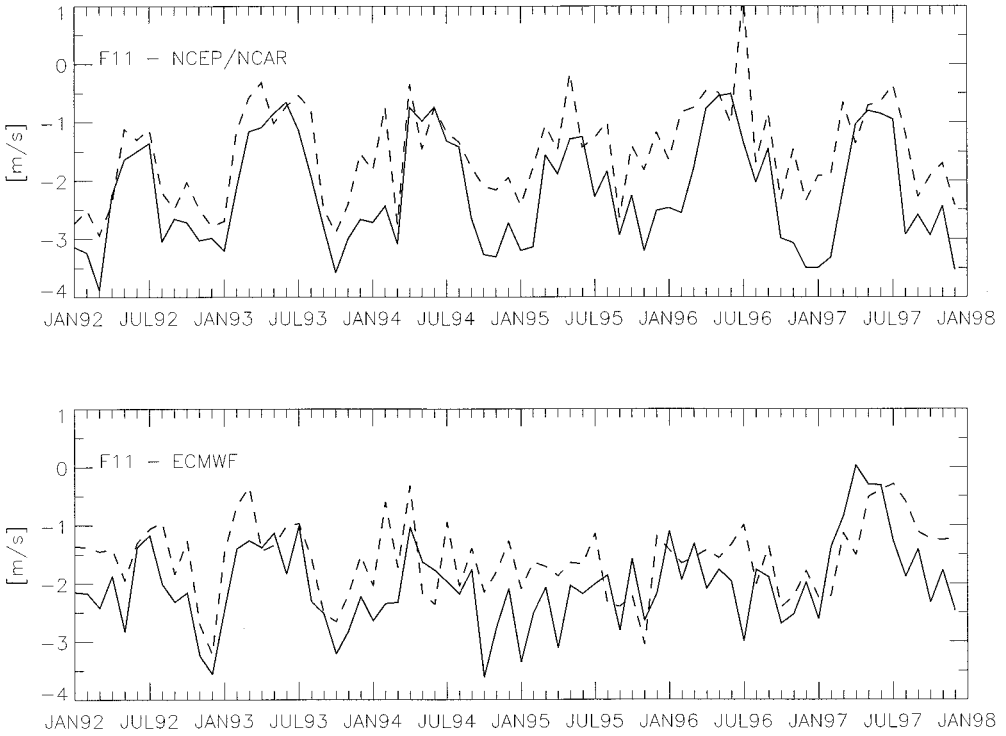

Figure 6. Monthly averaged wind speed differences for a 1° × 1° pixel centered at 11°E, 25°S (SW Africa): morning overpass (solid line) and evening overpass (dashed line).

implemented in May 1989 and September 1991. We have confirmed their observation from analysis of the time series and maps for satellite F08 between July 1987 and December 1991. Noticeable biases between F11 and ECMWF still remain during winter (January), which is again confirmed by the time series (Figure 4). However, the SSM/I − NSCAT map also shows a positive bias in this region during January, which is of the same size as the SSM/I − ECMWF bias. We therefore suspect that SSM/I overestimates the wind speeds in the tropical regions during the winter months.

In the southern extratropical eastern and central Pacific the SSM/I winds are too high compared with the analyses winds. The effect is strongest during fall and winter, when the biases exceed 2 m s^{-1} and are clearly visible in the SSM/I − NSCAT difference map.

The seasonal variations of the F11 − NCEP/NCAR wind speed biases at high northern latitudes, highlighted in the time series discussion, are also in Plate 1. At high southern latitudes (≥45°S) negative biases between SSM/I and the analyses occur in certain areas. The wind speed differences are between −0.5 and −1.5 m s^{-1} in the southern Atlantic Ocean, the Indian Ocean, and the western Pacific Ocean but not in the eastern and central Pacific Ocean. This may explain the overall low average wind speed differences in the (80°–30°S) latitudinal band time series. At this point we cannot determine if the effect originates from the SSM/I data or from the analyses data. The analyses data may lack necessary input since there are few in situ measurements in this region.

A persistent and relatively large negative bias exists off the Argentinean coast. The bias between SSM/I winds and both analyses wind speeds can be as large as −2 m s^{-1}. The wind speed differences are of greatest magnitude during summer and fall. The region lies in the southern westerl wind zone and is characterized by offshore westerly winds whose speeds are ~2–3 m s^{-1} lower than the zonal averages. We are presently not able to determine the cause of this bias. The ECMWF analysis persistently underestimates the wind speeds near the southern Pacific islands NE of Australia. Here the SSM/I − ECMWF bias reaches values of 3 m s^{-1} or more.

4.3. Description of Specific Coastal Regions

Finally, we want to point to a number of coastal regions where the collocated maps described above show rather large (up to −3 m s^{-1}) negative biases between SSM/I and analyses wind speeds. The biases in each of these locations vary by season. They are also visible in the F10E − NSCAT maps (Figure 6). The regions include (1) west of Namibia, Atlantic Ocean, strongest during fall and winter; (2) west of Mauritania, Atlantic Ocean, strongest during spring and summer; (3) west of Peru, Pacific Ocean, strongest during summer and fall, smaller size and intensity than regions 1 and 2; (4) west of California, Pacific Ocean, strongest during spring and summer; and (5) Arabian Sea, very strong during the summer months, effect previously noted by *Halpern et al.* [1994] and *Boutin et al.* [1996].

Separate maps were analyzed consisting of mean wind speed differences derived from ascending and descending SSM/I-analyses collocated data. These maps showed the biases are larger for the morning overpasses (descending) in the Southern Hemisphere (regions 1 and 3) and larger for the evening overpasses (ascending) in the Northern Hemisphere (regions 2 and 4). This explains why regions 2 and 4 appear stronger in the F10E-NSCAT map (Plate 4).

The four coastal regions (1–4) have common geographical characteristics. Each region lies at the transition between westerly winds and the trade wind zone located close to the coast

Table 2. Average Wind Speeds for a 1° × 1° Pixel Centered at 11°E, 25°S (SW Africa)[a]

	Wind Speed, m s^{-1}
F10E	7.79
NSCAT	8.39
NCEP/NCAR	8.86
ECMFW	8.68
COADS	8.74

[a]Wind speeds determined for September 1996 to June 1997. NSCAT, NCEP/NCAR reanalysis, and ECMWF data are collocated to F10E. COADS data are monthly averages and are not time collocated.

leading to a wind flow predominantly parallel to the coastline. The geography and wind patterns in these regions lead to the formation of equatorward eastern boundary currents flowing along the coast: (1) the Benguela current, (2) the Canary current, (3) the Humboldt (Peru) current, and (4) the California current. These currents are associated with upwelling of cold subsurface water near the coast, which results in a relatively large deviation of the sea surface temperature (SST) from the zonal mean [*Hartmann*, 1994]. A closer look at the maps reveals that the exact location of each of the four regions moves north to south along the coastline following the seasonal movement of the trade wind zone. In the Arabian Sea (region 5), during the summer months, strong monsoon winds blow along the coastline, which drive the flow of strong monsoon current along the coast and are associated with cold SST. In all five regions the largest biases are observed when the wind direction parallels the direction of the current.

For a more detailed investigation we chose to study one of these: region 1, west of Namibia in the Atlantic Ocean. A 1° × 1° pixel centered at 11°E, 25°S) was selected, and a time series was calculated for the F11-NCEP/NCAR and F11-ECMWF local morning and local evening collocated biases. Figure 6 shows that the biases exist in both the morning and evening data. If averaged over the whole time period, the bias in the morning overpass is ~0.7 m s^{-1} stronger. As we mentioned earlier, the situation is reversed for regions 2 and 4 in the Northern Hemisphere. The predominant wind direction in regions 2 and 4 is north to south, whereas in regions 1 and 3 it is south to north. Because the F11 instrument is looking forward, we conclude that the bias is stronger in the upwind direction than in the downwind direction. This coincides with the systematic −1 m s^{-1} wind speed bias previously reported by *Wentz* [1997] for data within ±20° of upwind. Figure 6 also shows that the negative biases peak during late fall and are weakest in late spring. The reason for this is that; as mentioned earlier, the location of the largest bias is moving north and south along the coastline following the annual movement of the trade wind zone. Therefore the overlap of this location with the chosen 1° × 1° pixel is also changing with the seasons.

The wind speed biases in this pixel over the whole time period between 1992 and 1997 are $\langle \bar{W} \rangle_{F11} - \langle \bar{W} \rangle_{NCEP} = 1.87$ m s^{-1} and $\langle \bar{W} \rangle_{F11} - \langle \bar{W} \rangle_{ECMWF} = 1.80$ m s^{-1}, respectively. From section 3.2 we know the global biases over this time period, which are $(\langle \bar{W} \rangle_{F11} - \langle \bar{W} \rangle_{NCEP})_{global} = +0.51$ m s^{-1} and $(\langle \bar{W} \rangle_{F11} - \langle \bar{W} \rangle_{ECMWF})_{global} = +0.40$ m s^{-1}, respectively. The standard deviation is ~1.0 m s^{-1} in both cases if the sample spaces consist of long time averages in each 1° pixel. This means that the deviations between the local and the global biases are at least at the 2.2σ level in both cases. Table 2 contains the time collocated wind speeds for the 1° pixel averaged between September 1996 and June 1997 for F10E, NSCAT, NCEP, and ECMWF. For comparison, we have included the NCEP real-time marine data set average wind speed derived from Comprehensive Ocean-Atmosphere Data Set (COADS) ship observations [*Woodruff et al*., 1993], even though the value is not time collocated to the satellite data. Furthermore, the COADS average is based on roughly half as many data as the number of satellite collocations per month. We use the values for the global mean and standard deviations from Table 1 as a reference and determine the deviations of the local from the global biases. We find 1.8σ for F10E − NSCAT, 1.6σ for F10E – NCEP/NCAR, and 1.7σ for F10E − ECMWF. On the other hand, the differences for all the other measurements are much smaller: 0.8σ for NSCAT − NCEP/NCAR and 0.5σ for NSCAT-ECMWF. Note that only evening overpass (ascending orbit) data are used in the NSCAT comparison. Therefore a pixel in the Southern Hemisphere has a downwind look direction and a weaker observable bias than for the morning overpass (descending orbit and upwind look direction) data. We conclude that part of the bias (about −1 m s^{-1}) showing in the wind speed difference maps can be attributed to the known wind error for upwind SSM/I observations [*Wentz*, 1997]. Table 2 exhibits therefore the residual bias between the SSM/I and all the other observations after subtracting this upwind error. As we can see, his bias is significant at the 1.6σ–1.8σ level. In other words, given the global values from Table 1, the probability that the low local mean values of the SSM/I observations in Table 2 occur by chance just within one pixel is 10% or less. The probability that it occurs accidentally in two or more coherent pixels of this size is already extremely small. As one can see from the maps (Plates 1, 2, and 4), the effect comprises several pixels.

At this time we do not know the cause of these large regional biases beyond the upwind error. We suspect that it might be connected with the flow of the ocean surface currents parallel to the coast and parallel to the predominant wind direction, which might influence the formation of surface waves. It should be noted that the radiometer does not measure the wind speed directly but rather measures the roughness of the sea surface. It is mainly sensitive to large gravity waves that are produced by the stress of the wind on the ocean surface. Another possible cause might be the cold SST, which is associated with the currents. Unusual conditions such as currents or cold SST could lead to inaccuracies in the radiative transfer model function for the brightness temperatures $T_{B_{model}}$. This radiative transfer model function has been primarily empirically derived and is the basis of the SSM/I retrieval algorithm [*Wentz*, 1997]. Possible inaccuracies in this model function at certain conditions (e.g., currents or cold SST) could therefore influence the SSM/I retrievals when those conditions are present. We intend to perform a more detailed study of this effect, which also includes data from the Tropical Rainfall Measurement Mission Microwave Imager (TMI) radiometer. The TMI instrument contains two lower-frequency channels (10 GHz v and h pol), allowing simultaneous retrieval of SST and wind speed [*Wentz et al*., 2000]. Moreover, it will help us to decide whether the effect appears only with the SSM/I instrument or also with other radiometers.

A recent analysis performed by *Liu et al* [1998] compared winds from NSCAT and ECMWF and identified a problem with the ECMWF wind directions at regions 1 and 3. The effect that they observe is mainly a difference in the wind

direction and not the wind speed as presented in our study. They find a large difference in the zonal (E–W) wind components in the regions 1 and 3 in the Southern Hemisphere, and they also report the seasonal north to south annual movement of these regions with the southern trade wind zone. They conclude that the ECMWF winds are missing the continental influence in these regions. However, they do not identify any of the Northern Hemisphere (regions 2, 4, and 5 presented here).

5. Summary and Conclusions

Our investigation compares ocean surface wind speeds from four SSM/I satellites with those obtained from the NCEP/NCAR reanalysis and the ECMWF/TOGA Global Analysis over a time period from 1988 to 1997. The study comparison performed between F11 SSM/I and the analyses data is presented in this paper as representative of results obtained for F08, F10, and F13 SSM/I. In addition, we present a comparison of 10 months of F10 SSM/I wind speeds to NSCAT wind speeds. NSCAT data available from September 1996 to June 1997 are used to highlight observed regional biases and to decide if the SSM/I data algorithm or the analyses are the sources of the observed biases.

The standard deviations of the SSM/I − analyses wind speed differences are 2.1 m s^{-1} in case of the ECMWF analysis and 2.4 m s^{-1} in case of the NCEP/NCAR reanalysis if all collocated events are considered. If monthly or yearly time averages in each pixel are used, the values are 0.8 and 1.2 m s^{-1}, respectively. With the exception of F10M SSM/I the changes of the differences in the measured wind speeds for a specific satellite over time are small. We identify a drift in the morning overpass F10 SSM/I satellite data. This drift may be due to the progression of the F10 ascending crossing time throughout the 6 year operational period. In addition, we find that the differences among the various SSM/I satellites are small. They are due to small intercalibration errors. After subtracting these intercalibration offsets we find that the global average of winds measured by SSM/I is ~7.3 m s^{-1}. The global average analyses wind speeds are on average between 0.2 and 0.3 m s^{-1} lower than the satellite wind speed average.

Our study describes local biases in several geographical regions. These bias regions include (1) low NCEP/NCAR reanalysis wind speeds in the eastern tropical Pacific and tropical Atlantic, although during winter the SSM/I winds are presumably too high in this region; (2) low ECMWF wind speeds within southern Pacific islands NE of Australia; (3) high SSM/I wind speeds in the extratropical southern central and eastern Pacific during fall and winter; (4) a negative bias between SSM/I and analyses wind speeds off the Argentinean coast, whose cause is presently unknown, and (5) seasonal low SSM/I wind speeds at five coastal regions (West of Namibia, West of Mauritania, West of Peru, West of of California, and the Arabian Sea). Each of these coastal regions was also located in the F10E − NSCAT wind speed difference maps. Part of the bias can be attributed to a known upwind error of −1.0 m s^{-1} in the SSM/I wind retrieval, though a substantial effect remains. Ocean currents flowing in these regions may contribute to the effect.

Notation

W scalar wind speed, m s^{-1}.

$\langle W \rangle = \frac{1}{N}\sum_{i=1}^{N} W_i$ mean (average of W, sample size N (large), W_i, $i = 1, \ldots, N$ samples.

$\sigma(W) = \sqrt{\frac{1}{N}\sum_{i=1}^{N}(W_i - \langle W \rangle)^2} = \sqrt{\langle W^2 \rangle - \langle W \rangle^2}$ standard deviation of W.

$\bar{W}$ Time average (month, year) taken in each pixel.

$\sigma(\bar{W})$ Standard deviation after taking time average in each pixel.

Fxx SSM/I satellites, xx = 08, 10, 11, or 13.

FxxM morning overpass of SSM/I satellite Fxx.

FxxE evening overpass of SSM/I satellite Fxx.

Acknowledgments. This research was funded by NASA grant NAG5-6642, Oregon State University subcontract NS070-01, NASA task order RF-225, Jet Propulsion Laboratory subcontract 960644, NASA cooperative agreement NCC8-141, University of Alabama at Huntsville subcontract SUB1998-101, and NASA contract NASW-5038. The NCEP/NCAR and ECMWF data sets were supplied by NCAR's Data Support Section. We would like to thank Chi-Fan Shih (NCAR) for providing FORTRAN routines used to read the GRIB data sets.

References

Boutin, J., L. Siefridt, J. Etcheto, and B. Barnier, Comparison of ECMWF and satellite ocean wind speeds from 1985 to 1992, *Int. J. Remote Sens.*, *17*, 2987–2913, 1996.

Dunbar, S., *NASA Scatterometer: High-Resolution Merged Geophysical Data Product (User's Guide)*, Jet Propul. Lab., Pasadena, Calif., 1997.

European Centre for Medium-Range Weather Forecasts (ECMWF), *The Description of the ECMWF/WCRP Level II-A Global Atmospheric Data Archive*, Reading, Engl., U.K., 1993.

Halpern, D., A. Hollingsworth, and F. Wentz, ECMWF and SSM/I global surface wind speeds, *J. Atmos. Oceanic Technol.*, *11*, 779–788, 1994.

Hartmann, D. L., *Global Physical Climatology*, Academic, San Diego, Calif., 1994.

Kalnay, E., M. Kanamitsu, R. Kistler, W. Collins, D. Deaven, L. Gandin, and M. Iredell, The NCEP/NCAR 40-year reanalysis project, *Bull. Am. Meteorol. Soc.*, *77*, 437–471, 1996.

Krasnopolsky, V. M., B. L. C., and W. H. Gemmill, A neural network as a nonlinear transfer function model for retrieving surface wind speeds from the SSM/I, *J. Geophys. Res.*, *100*, 11,033–11,045, 1995.

Liu, W. T., W. Tang, and P. S. Polito, NASA scatterometer provides global ocean-surface wind fields with more structures than numerical weather prediction, *Geophys. Res. Lett.*, *2*, 761–764, 1998.

Mears, C. A., D. K. Smith, and F. J. Wentz, Comparison of Special Sensor Microwave Imager and buoy-measured wind speeds from 1987 to 1997, *J. Geophys. Res.*, this issue.

Wells, N., *The Atmosphere and Ocean*, John Wiley, New York, 1997.

Wentz, F. J., A well-calibrated ocean algorithm for Special Sensor Microwave/Imager, *J. Geophys. Res.*, *102*, 8703–8718, 1997.

Wentz, F. J., and D. K. Smith, A model function for the ocean normalized radar cross section at 14 GHz derived from NSCAT observations, *J. Geophys. Res.*, *104*, 11,499–11,514, 1999.

Wentz, F., C. Gentemann, D. Smith, and D. Chelton, Satellite measurements of sea surface temperature through clouds, *Science*, *288*, 847–850, 2000.

Wilks, D., *Statistical Methods in the Atmospheric Sciences*, Academic, San Diego, Calif., 1995.

Woodruff, S. D., S. J. Lubker, K. Wolter, S. J. Worley, and J. D. Elms, Comprehensive Ocean-Atmosphere Data Set (COADS) release 1a: 1980–92, *Earth Syst. Monit.*, *4*, 1–8, 1993.

T. Meissner, D. Smith, and F. Wentz, Remote Sensing Systems, 438 First Street, Suite 200, Santa Rosa, CA 95401. (meissner@remss.com)

(Received October 12, 1999; revised November 8, 2000; accepted January 10, 2001.)